Fracture Analysis of Functionally Graded Materials by a BEM

X.W. Gao, Ch. Zhang, J. Sladek, V. Sladek

Fracture Analysis of Functionally Graded Materials by a BEM

X.W. Gao, Ch. Zhang, J. Sladek, V. Sladek

PII: S0266-3538(07)00350-8
DOI: 10.1016/j.compscitech.2007.08.029
Reference: CSTE 3821

To appear in: *Composites Science and Technology*

Received Date: 16 May 2007
Revised Date: 9 August 2007
Accepted Date: 31 August 2007

Please cite this article as: Gao, X.W., Zhang, Ch., Sladek, J., Sladek, V., Fracture Analysis of Functionally Graded Materials by a BEM, *Composites Science and Technology* (2007), doi: 10.1016/j.compscitech.2007.08.029

Fracture Analysis of Functionally Graded Materials by a BEM

X. W. Gao[a], Ch. Zhang[b,*], J. Sladek[c] and V. Sladek[c]

[a] *Department of Engineering Mechanics, Southeast University, Nanjing, PR China*

[b] *Department of Civil Engineering, University of Siegen, D-57068 Siegen, Germany*

[c] *Institute of Construction and Architecture, Slovak Academy of Sciences, 84503 Bratislava, Slovakia*

Keywords: A. Functional composites; B. Fracture; B. Mechanical properties; C. Crack; C. Computational mechanics

Abstract. In this paper, crack analysis in two-dimensional (2-D), continuously nonhomogeneous, isotropic and linear elastic functionally graded materials (FGMs) is presented. For this purpose, a boundary element method (BEM) based on a boundary-domain integral equation formulation is developed. An exponential variation with spatial variables is assumed for Young's modulus of the FGMs, while a constant Poisson's ratio is considered. Fundamental solutions for homogeneous, isotropic and linear elastic solids are applied in the formulation. To avoid displacement gradients in the domain-integral, normalized displacements are introduced. By using the radial integration method, the domain-integral is transformed into boundary integrals over the global boundary. The normalized displacements in the domain-integral are approximated by a combination of radial basis functions and polynomials in terms of global coordinates, which leads to a meshless scheme. Special attention of the analysis is devoted to the computation of the most important crack-tip characterizing parameters of cracked FGMs, namely the stress intensity factors. To show the effects of the material

gradation on the stress intensity factors, numerical examples are presented and discussed.

1. Introduction

In recent years, a new class of composite materials, the so-called functionally graded materials (FGMs), attracted many research interests in materials and engineering sciences [1,2]. FGMs are advantageous over classical homogeneous materials with only one material constituent, because FGMs consist of more material constituents and they combine the desirable properties of each constituent. As a representative example for FGMs, we just mention the metal/ceramic FGMs, which are compositionally graded from a ceramic phase to a metal phase. Metal/ceramic FGMs can incorporate advantageous properties of both ceramics and metals such as the excellent heat, wear, and corrosion resistances of ceramics and the high strength, high toughness, good machinability and bonding capability of metals without severe internal thermal stresses. However, ceramics have a brittle nature, and microcracks or crack-like defects are often induced in the fabrication process or under the in-service loading conditions. Thus, fracture and fatigue analysis of FGMs is an important research issue to the design, optimization, and novel engineering applications of FGMs. For cracked FGMs with general geometry and loading conditions, advanced numerical methods have to be applied, because of the high mathematical complexity of the corresponding governing partial differential equations with variable coefficients, and because the most available analytical methods can be successfully applied to cracked FGMs only with very simple geometry and loading conditions. In this context, we just mention the singular integral equation method [3-7], the classical finite element method (FEM) [8-15], the graded

finite element method [16-19], the extended finite element method (XFEM) [20], the element-free Galerkin method (EFG) [21,22], the boundary integral equation method (BIEM) or boundary element method (BEM) [23-27], and the meshless Petrov-Galerkin method (MLPG) [28-31].

Although the BEM has been successfully applied to homogeneous, isotropic and linear elastic solids for many years, its application to FGMs is yet very limited due the fact that the corresponding fundamental solutions or Green's functions for general FGMs are either not available or mathematically too complex [32,33]. The nonhomogeneous nature of FGMs prohibits an easy construction and implementation of fundamental solutions for general FGMs.

In this paper, crack analysis in 2-D, continuously nonhomogeneous, isotropic and linear elastic FGMs is presented. For this purpose, a boundary-domain integral equation formulation is applied. For simplicity, an exponential variation of Young's modulus and constant Poisson's ratio are assumed. Fundamental solutions for homogeneous, isotropic and linear elastic solids are applied in the present formulation, which results in a boundary-domain integral equation formulation due to the materials nonhomogeneity. To avoid displacement gradients in the domain integral, normalized displacements are introduced. The radial integration method of Gao [34,35] is applied to convert the arising domain-integral into boundary-integrals over the global boundary of the cracked solids. Basis functions consisting of a combination of radial basis functions and polynomials in terms of global coordinates are used to approximate the normalized displacements in the domain-integral. In this manner, a meshless scheme is obtained, which requires only conventional boundary discretization and additional interior nodes instead of cells or meshes. An advantage of the present BEM is that it is easy to

implement and can be easily incorporated into an existing BEM code for homogeneous, isotropic and linear elastic solids. Special attention of the analysis is devoted to the investigation of the material gradation on the stress intensity factors. Numerical examples for cracks parallel and perpendicular to the material gradation are presented and discussed.

2. Boundary-Domain Integral Equations

We consider 2-D, continuously nonhomogeneous, isotropic and linear elastic FGMs. In the absence of body forces, the equilibrium equations are given by

$$\sigma_{ij,j} = 0\,, \tag{1}$$

where σ_{ij} represents the stress tensor, a comma after a quantity represents spatial derivatives and repeated indexes denote summation. It is assumed that the Young's modulus $E(\boldsymbol{x})$ of the FGMs depends on Cartesian coordinates while Poisson's ratio ν is constant. In this case, the elasticity tensor $C_{ijkl}(\boldsymbol{x})$ can be written as

$$C_{ijkl}(\boldsymbol{x}) = \mu(\boldsymbol{x}) C^0_{ijkl}\,, \tag{2}$$

where

$$\mu(\boldsymbol{x}) = \frac{E(\boldsymbol{x})}{2(1+\nu)}, \qquad C^0_{ijkl} = \frac{2\nu}{1-2\nu}\delta_{ij}\delta_{kl} + \delta_{ik}\delta_{jl} + \delta_{il}\delta_{jk}\,. \tag{3}$$

In Eqs. (2) and (3), $\mu(\boldsymbol{x})$ denotes the shear modulus and δ_{ij} represents the Kronecker delta.

The stress tensor σ_{ij} and the displacement gradients $u_{k,l} = \partial u_k / \partial x_l$ are related by the generalized Hooke's law

$$\sigma_{ij} = C_{ijkl} u_{k,l} = \mu(\boldsymbol{x}) C^0_{ijkl}\, u_{k,l}\,. \tag{4}$$

The traction vector t_i on the boundary of the considered domain is related to the stress components by

$$t_i = \sigma_{ij} n_j , \tag{5}$$

where n_j is the outward unit normal vector to the boundary Γ of the domain Ω.

The weak-form of the equilibrium equations (1) can be written as

$$\int_{\Omega} \sigma_{jk,k} \cdot U_{ij} d\Omega = 0 , \tag{6}$$

where $U_{ij}(\boldsymbol{x}, \boldsymbol{y})$ is the weight or test function. Substitution of Eq. (4) into Eq. (6) and application of Gauss's divergence theorem yield

$$\int_{\Gamma} U_{ij} t_j d\Gamma - \int_{\Gamma} T_{ij} \mu u_j d\Gamma + \int_{\Omega} C^0_{rsjl} U_{ir,sl} \mu u_j d\Omega + \int_{\Omega} C^0_{rsjl} U_{ir,s} \mu_{,l} u_j d\Omega = 0 , \tag{7}$$

where

$$T_{ij} = \Sigma_{ijl} n_l , \tag{8}$$

$$\Sigma_{ijl} = C^0_{rsjl} U_{ir,s} = \frac{2\nu}{1-2\nu} U_{ik,k} \delta_{jl} + U_{ij,l} + U_{il,j} . \tag{9}$$

For the weight function $U_{ij}(\boldsymbol{x}, \boldsymbol{y})$, we choose the displacement fundamental solutions for homogeneous, isotropic and linear elastic solids, which satisfy the following partial differential equations

$$C^0_{rsjl} U_{ir,sl} = -\delta_{ij} \delta(\boldsymbol{x} - \boldsymbol{y}) , \tag{10}$$

where $\delta(\boldsymbol{x} - \boldsymbol{y})$ is the Dirac delta function. The solution $U_{ij}(\boldsymbol{x}, \boldsymbol{y})$ of Eq. (10) is given by the Kelvin's displacement fundamental solutions for homogeneous, isotropic and linear elastic solids with μ=1, which can be written as [36]

$$U_{ij} = -\frac{1}{8\pi(1-\nu)}\left[(3-4\nu)\delta_{ij}\ln(r) - r_{,i}r_{,j}\right], \tag{11}$$

where $r = |\boldsymbol{x} - \boldsymbol{y}|$. Substitution of Eq. (10) into Eq. (7) and application of the sifting property of the Dirac delta function lead to

$$\tilde{u}_i(\boldsymbol{y}) = \int_\Gamma U_{ij}(\boldsymbol{x},\boldsymbol{y})t_j(\boldsymbol{x})d\Gamma - \int_\Gamma T_{ij}(\boldsymbol{x},\boldsymbol{y})\tilde{u}_j(\boldsymbol{x})d\Gamma + \int_\Omega V_{ij}(\boldsymbol{x},\boldsymbol{y})\tilde{u}_j(\mathbf{x})d\Omega, \tag{12}$$

where the normalized displacements $\tilde{u}_i(\boldsymbol{x})$ and the normalized shear modulus $\tilde{\mu}(\boldsymbol{x})$ are defined by

$$\tilde{u}_i(\boldsymbol{x}) = \mu(\boldsymbol{x})u_i(\boldsymbol{x}), \tag{13}$$

$$\tilde{\mu}(\boldsymbol{x}) = \log\mu(\boldsymbol{x}). \tag{14}$$

The fundamental solutions $T_{ij}(\boldsymbol{x},\boldsymbol{y})$ and $V_{ij}(\boldsymbol{x},\boldsymbol{y})$ arising in Eq. (12) can be expressed as [36]

$$\Sigma_{ijl} = -\frac{1}{4\pi(1-\nu)r}\left[(1-2\nu)\left(\delta_{il}r_{,j} + \delta_{ij}r_{,l} - \delta_{jl}r_{,i}\right) + 2r_{,i}r_{,j}r_{,l}\right], \tag{15}$$

$$T_{ij} = \Sigma_{ijl}n_l = -\frac{1}{4\pi(1-\nu)r}\left[(1-2\nu)\left(n_i r_{,j} - n_j r_{,i}\right) + \left((1-2\nu)\delta_{ij} + 2r_{,i}r_{,j}\right)r_{,l}n_l\right], \tag{16}$$

$$V_{ij} = \Sigma_{ijl}\tilde{\mu}_{,l} = -\frac{1}{4\pi(1-\nu)r}\left[(1-2\nu)\left(\tilde{\mu}_{,i}r_{,j} - \tilde{\mu}_{,j}r_{,i}\right) + \left((1-2\nu)\delta_{ij} + 2r_{,i}r_{,j}\right)r_{,l}\tilde{\mu}_{,l}\right]. \tag{17}$$

Boundary-domain integral equations for boundary points can be obtained by letting $\boldsymbol{y} \to \Gamma$ in Eq. (12). It should be remarked here that the boundary-domain integral equations (12) are formulated in terms of the boundary tractions t_j and the normalized displacements $\tilde{u}_j$ in contrast to most previous boundary-domain integral equation formulations for nonhomogeneous, isotropic and linear elastic solids, where

displacement gradients arise in the domain-integral. This feature not only facilitates the numerical implementation, but also leads to a high accuracy of the computational method. In the case of an exponential law for Young's modulus or shear modulus such as that used in this analysis, it can be seen from Eq. (14) that $\tilde{\mu}_{,i}$ is constant and $V_{ij}(\boldsymbol{x},\boldsymbol{y})$ thus becomes very simple for integration.

3. Numerical Solution Procedure

The boundary discretization of the boundary-domain integral equations (12) can be done by following the usual procedure applied in the conventional BEM. A key issue to the numerical solution procedure is how to compute the domain integral in (12). Compared to the classical mesh- or cell-integration method, a transform of the domain-integral in (12) into boundary integrals over the global boundary is advantageous. In this paper, the radial integration method (RIM) of Gao [34,35] is used for this purpose. In the RIM, the normalized displacements in the domain-integral of Eq. (12) are approximated by a series of prescribed basis functions as used in the dual reciprocity method [37]. Previous including our own investigations have demonstrated that a combination of the radial basis functions and the polynomials in terms of global coordinates is very promising (see e.g. [38] for more details). For this reason, the normalized displacements $\tilde{u}_i(\boldsymbol{x})$ are approximated by

$$\tilde{u}_i(\boldsymbol{x}) = \sum_A \alpha_i^A \phi^A(R) + a_i^k x_k + a_i^0 , \tag{18}$$

$$\sum_A \alpha_i^A = 0 , \qquad \sum_A a_i^A x_j^A = 0 , \tag{19}$$

where $\phi^A(R)$ is he radial basis function, $R=\left\|\boldsymbol{x}-\boldsymbol{x}^A\right\|$ is the distance from the application point A to the filed point $\boldsymbol{x}$, α_i^A and a_i^k are unknown coefficients to be determined, and x_j^A denotes the coordinates at the application point A which consists of all boundary nodes and some internal points. In this analysis, the following 4-th order spline-type radial basis function is applied

$$\phi^A(R)=\begin{cases}1-6\left(\dfrac{R}{d_A}\right)^2+8\left(\dfrac{R}{d_A}\right)^3-3\left(\dfrac{R}{d_A}\right)^4, & 0\le R\le d_A,\\ 0, & R\ge d_A,\end{cases} \tag{20}$$

where d_A is the support size for the application point A.

The unknown coefficients α_i^A and a_i^k in Eq. (18) can be determined by applying the application point A in Eqs. (18) and (19) to every node. Then, a set of linear algebraic equations can be obtained as

$$\tilde{\boldsymbol{u}}=\boldsymbol{\phi}\cdot\boldsymbol{\alpha}, \tag{21}$$

where $\boldsymbol{\alpha}$ is a vector containing the coefficients α_i^A for all application points and a_i^k. If two nodes do not coincide, the matrix $\boldsymbol{\phi}$ is invertible and therefore

$$\boldsymbol{\alpha}=\boldsymbol{\phi}^{-1}\cdot\tilde{\boldsymbol{u}}. \tag{22}$$

Substitution of Eq. (18) into the domain-integral of Eq. (12) results in

$$\int_\Omega V_{ij}\tilde{u}_j d\Omega=\alpha_j^A\int_\Omega V_{ij}\phi^A d\Omega+a_j^k\int_\Omega V_{ij}x_k d\Omega+a_j^0\int_\Omega V_{ij}d\Omega. \tag{23}$$

The domain-integrals in Eq. (23) can be transformed into boundary integrals by using RIM [34,35] as

$$\int_\Omega V_{ij}\tilde{u}_j d\Omega=\alpha_j^A\int_\Gamma\frac{1}{r}\frac{\partial r}{\partial n}F_{ij}^A d\Gamma+a_j^k\int_\Gamma\frac{r_{,k}}{r}\frac{\partial r}{\partial n}F_{ij}^1 d\Gamma+\left(a_j^k y_k+a_j^0\right)\int_\Gamma\frac{1}{r}\frac{\partial r}{\partial n}F_{ij}^0 d\Gamma, \tag{24}$$

where

$$F_{ij}^{A} = \int_0^r rV_{ij}\,\phi^{A} dr\,, \qquad F_{ij}^{1} = \int_0^r r^2 V_{ij}\, dr\,, \qquad F_{ij}^{0} = \int_0^r rV_{ij}\, dr\,. \tag{25}$$

It should be noted here that in the radial integrals of Eq. (24), the term $r_{,i}$ is constant and the relation

$$x_i = y_i + r_{,i}\, r \tag{26}$$

is used for the transformation from $\boldsymbol{x}$ to r. The last two radial integrals in Eq. (25) can be evaluated analytically. The first radial integral in Eq. (25) is regular and can be computed numerically by using standard Gaussian quadrature formula. To this end, the function $\phi^{A}(R)$ should be expressed as a function of r, which can be done by using the following relation (see Fig. 1)

$$R = \sqrt{r^2 + sr + \bar{R}^2}\,, \tag{27}$$

where

$$s = 2r_{,i}\bar{R}_i\,, \tag{28}$$

$$\bar{R} = \left|\boldsymbol{y} - \boldsymbol{x}^{A}\right| = \sqrt{\bar{R}_i \cdot \bar{R}_i}\,, \tag{29}$$

$$\bar{R}_i = y_i - x_i^{A}\,. \tag{30}$$

After numerical integrations and substitution of Eq. (22) into Eq. (24), an expression for the domain-integral in terms of the normalized displacement vector $\tilde{\boldsymbol{u}}$ at all nodes can be obtained. If the BEM model consists of N_b boundary nodes and N_i internal nodes and after invoking the boundary conditions, the boundary-domain integral equations (12) lead to the following system of linear algebraic equations

$$\boldsymbol{A}_b \cdot \boldsymbol{x}_b = \boldsymbol{y}_b + \boldsymbol{V}_b \cdot \tilde{\boldsymbol{u}}, \qquad \text{for boundary nodes,} \tag{31}$$

$$\tilde{\boldsymbol{u}}_i = \boldsymbol{A}_i \cdot \boldsymbol{x}_b + \boldsymbol{y}_i + \boldsymbol{V}_i \cdot \tilde{\boldsymbol{u}}, \qquad \text{for internal nodes.} \tag{32}$$

In Eqs. (31) and (32), the sizes of the matrices $\boldsymbol{A}_b$ and $\boldsymbol{A}_i$ are $2N_b \times 2N_b$ and $2N_i \times 2N_b$, while $\boldsymbol{V}_b$ and $\boldsymbol{V}_i$ are $2N_b \times 2N_t$ and $2N_i \times 2N_t$ with $N_t = N_b + N_i$, respectively. The vector $\boldsymbol{x}_b$ with a size of $2N_b \times 1$ contains the unknown normalized boundary displacements or the unknown boundary tractions, while the vector $\tilde{\boldsymbol{u}}$ with a size of $2N_t \times 1$ consists of the unknown normalized boundary displacements and all normalized internal displacements. It should be noted here that after invoking the boundary conditions, the columns of the matrices $\boldsymbol{V}_b$ and $\boldsymbol{V}_i$ corresponding to the known boundary displacement nodes should be taken as zero.

Equations (31) and (32) can be written in a more compact form as

$$\left(\begin{bmatrix} \boldsymbol{A}_b & \boldsymbol{0} \\ -\boldsymbol{A}_i & \boldsymbol{I} \end{bmatrix} - \begin{bmatrix} \boldsymbol{V}_b \\ \boldsymbol{V}_i \end{bmatrix} \right) \begin{Bmatrix} \boldsymbol{x}_b \\ \tilde{\boldsymbol{u}}_i \end{Bmatrix} = \begin{Bmatrix} \boldsymbol{y}_b \\ \boldsymbol{y}_i \end{Bmatrix}, \tag{33}$$

where $\boldsymbol{I}$ is the identity matrix. From Eq. (33), both the boundary unknowns $\boldsymbol{x}_b$ and the normalized internal displacements $\tilde{\boldsymbol{u}}_i$ can be obtained numerically. Then, the true displacements can be obtained by using Eq. (13). Subsequently, the stresses at internal points can be computed by a usual data post-processing.

4. Computation of Stress Intensity Factors

Since the asymptotic crack-tip field for continuously nonhomogenous, isotropic and linear elastic solids has the same structure as that for homogeneous, isotropic and linear elastic solids [8], the stress intensity factors can be computed by using the following relations

$$\begin{Bmatrix} K_I \\ K_{II} \end{Bmatrix} = \frac{2\mu^{tip}}{\kappa+1}\sqrt{\frac{2\pi}{r}} \begin{Bmatrix} u_2(r,\pi) \\ u_1(r,\pi) \end{Bmatrix}, \tag{34}$$

$$\kappa = \begin{cases} 3-4\nu, & \text{plane strain,} \\ (3-\nu)/(1+\nu), & \text{plane stress,} \end{cases} \tag{35}$$

where r is the radial coordinate with the origin at the crack-tip, $u_1(r,\pi)$ and $u_2(r,\pi)$ are the crack-face displacements, μ^{tip} is the shear modulus at the crack-tip, and K_I and K_{II} are the mode-I and mode-II stress intensity factors. In this analysis, a least-squares technique based on the minimization of the quadratic deviations of the displacements on the crack-faces is used for computing the stress intensity factors. This technique leads to the following simple formula [39]

$$\begin{Bmatrix} K_I \\ K_{II} \end{Bmatrix} = \frac{1}{\sum_\alpha r_\alpha} \begin{Bmatrix} \sum_\alpha \left[\sqrt{r_\alpha} \cdot \hat{u}_2(r_\alpha) \right] \\ \sum_\alpha \left[\sqrt{r_\alpha} \cdot \hat{u}_1(r_\alpha) \right] \end{Bmatrix}, \tag{36}$$

where

$$\begin{Bmatrix} \hat{u}_1(r_\alpha) \\ \hat{u}_2(r_\alpha) \end{Bmatrix} = \frac{2\mu^{tip}}{\kappa+1}\sqrt{2\pi} \begin{Bmatrix} u_1(r_\alpha,\pi) \\ u_2(r_\alpha,\pi) \end{Bmatrix}, \tag{37}$$

in which the displacements at the discrete nodes r_α from the crack-tip are used.

5. Numerical Results

In the first numerical example, we consider an edge crack parallel to the material gradation in a rectangular FGM plate, which is subjected to a uniform tensile loading as depicted in Fig. 2. The geometry of the cracked plate is described by: plate width $b = 10$, plate length $2h = 30$ and crack-length $a = 0.4b$. The material gradation in the x_1-direction parallel to the crack is described by the an exponential law

$$E(x_1) = E_0 e^{\alpha x_1}, \qquad \alpha = \frac{1}{b}\ln\left(\frac{E_w}{E_0}\right), \tag{38}$$

with E_0 and E_w being the Young's modulus at the left and the right side of the plate. Poisson's ratio is taken as ν=0.25 and plane strain condition is assumed in the numerical calculations. Due to symmetry of the problem, only one half of the plate is considered. 180 boundary nodes and 251 internal nodes are used in the discretization. On the global boundary of the plate, 3-noded quadratic boundary elements are applied. To consider the stress concentration near the crack-tip, dense boundary and internal nodes are used as shown in Fig. 3.

To test the accuracy of the implemented BEM, the computed displacement component u_2 on the crack-face is compared with the FEM result in Fig. 4, which shows an excellent agreement between both results. Here, the Young's moduli are taken as $E_0 = 10000$ and $E_w = 50000$. In the FEM calculation, 900 cubic four-noded graded elements are applied, where a linear variation of Young's modulus within each element is assumed.

To investigate the sensitivity of the implemented BEM to the used number and distribution of internal nodes, numerical calculations with different node numbers and distributions have been also carried out. The number of boundary nodes (i.e., 180) has been taken as constant, while the number and the distribution of internal nodes have been varied. In particular, non-uniform node distribution with 112, 57, 17 and 0 internal nodes, and uniform node distribution with 112 and 55 internal nodes have been applied. Our numerical results have shown that some internal nodes are required to achieve a sufficient accuracy of the numerical results [40]. Otherwise the implemented BEM is

quite robust and insensitive with respect to the used number and distribution of internal nodes. Generally speaking, an increase in the number of internal nodes improves the accuracy of the present numerical method, but it may increase the required computing time drastically.

The normalized mode-I stress intensity factor $K_I / \sigma_{22}\sqrt{\pi a}$ versus the dimensionless gradient parameter αb is presented in Fig. 5. The normalized mode-I stress intensity factor decreases with increasing dimensionless gradient parameter αb. Here, the mode-II stress intensity factor is identically zero due to the symmetry of the problem with respect to the crack-line.

In the second numerical example, we consider an edge crack perpendicular to the material gradation in a rectangular functionally graded plate as depicted in Fig. 6. The cracked plate has the same geometry and loading condition as in the first numerical example. The material gradation in the x_2-direction perpendicular to the crack is described by an exponential law as

$$E(x_2) = E_0 e^{\beta x_2}, \qquad \beta = \frac{1}{2h}\ln\left(\frac{E_H}{E_0}\right), \tag{39}$$

with E_0 and E_H being the Young's modulus at the bottom and the top side of the cracked plate. Also here, Poisson's ratio is taken as ν=0.25 and plane strain condition is assumed in the numerical calculations. Young's modulus at the bottom side of the plate is fixed as $E_0 = 10000$, while Young's modulus at the bottom side of the plate is varied. For the discretization of the cracked plate, 139 boundary elements with 254 boundary nodes and 502 internal nodes are used. The node distribution is shown in Fig. 7.

Figures 8 and 9 show the influences of the dimensionless gradient parameter βh on the normalized mode-I and mode-II stress intensity factors $K_I / \sigma_{22}\sqrt{\pi a}$ and $K_{II} / \sigma_{22}\sqrt{\pi a}$. The normalized mode-I stress intensity factor has a minimum at $\beta h = 0$, which corresponds to a homogeneous plate, and it increases with increasing amplitude of the gradient parameter βh. The normalized mode-II stress intensity factor is zero in the case of a homogeneous plate (i.e., $\beta h = 0$), and its amplitude increases with increasing amplitude of the gradient parameter βh. This implies that the material gradation may affect the crack propagation direction, since the mode-II stress intensity factor has direct relevance to the direction of the crack propagation.

6. Conclusions

In this paper, fracture analysis of cracked FGMs by a BEM is presented. By using fundamental solutions for homogeneous, isotropic and linear elastic solids, a boundary-domain integral equation formulation is obtained. Normalized displacements are introduced to avoid displacement gradients in the domain-integral. A numerical solution procedure is developed to solve the boundary-domain integral equations. The domain-integral is transformed into boundary integrals over the global boundary of the considered domain by using the radial integration method of Gao [34,35]. The present method is a meshless method, which is suitable for crack analysis of 2-D continuously nonhomogeneous, isotropic and linear elastic FGMs. Numerical results show that the materials gradient may have significant influences on the stress intensity factors.

Acknowledgements

Support by the German Research Foundation (DFG) under the project number ZH 15/10-1 is gratefully acknowledged.

References

1. Suresh S, Mortensen A. Fundamentals of functionally graded materials. IOM Communications Ltd., London, 1998.
2. Miyamoto Y, Kaysser WA, Rabin BH, Kawasaki A, Ford RG (editors). Functionally graded materials. Kluwer Academic Publishers, Boston, 1999.
3. Delale F, Erdogan F. The crack problem for a nonhomogeneous plane. J Appl Mech 1983;50:609-614.
4. Erdogan F. The crack problem for bonded nonhomogeneous materials under antiplane shear loading. J Appl Mech 1985;52:823-828.
5. Erdogan F. Fracture mechanics of functionally graded materials. Composites Engineering 1995;5:753-770.
6. Konda N, Erdogan F. The mixed mode crack problem in a nonhomogeneous elastic medium. Eng Fract Mech 1994;47:533-545.
7. Chan YS, Paulino GH, Fannjiang AC. The crack problem for nonhomogeneous materials under antiplane shear loading - A displacement based formulation. Int J Solids Struct 2001;38:2989-3005.
8. Eischen JW. Fracture of nonhomogeneous materials. Int J Fract 1987;34:3-22.
9. Gu P, Asaro RJ. Cracks in functionally graded materials. Int J Solids Struct 1997;34:1-17.
10. Gu P, Asaro RJ. Crack deflection in functionally graded materials. Int J Solids Struct 1997;34:3085-3098.

11. Gu P, Dao M, Asaro RJ. A simplified method for calculating the crack tip field of functionally graded materials using the domain integral. J Appl Mech 1999;66:101-108.
12. Anlas G, Santare MH, Lambros J. Numerical calculation of stress intensity factors in functionally graded materials. Int J Fract 2000;104:131-143.
13. Marur PR, Tippur HV. Numerical analysis of crack-tip fields in functionally graded materials with a crack normal to the elastic gradient. Int J Solids Struct 2000;37:5353-5370.
14. Li H, Lambros J, Cheeseman BA, Santare MH. Experimental investigation of the quasi-static fracture of functionally graded materials. Int J Solids Struct 2000;37:3715-3732.
15. Zou ZZ, Wu SX, Li CY. On the multiple isoparametric finite element method and computation of stress intensity factor for cracks in FGMs. Key Eng Mater 2000;183-187:511-516.
16. Santare MH, Lambros J. Use of a graded finite element to model the behavior of nonhomogeneous materials. J Appl Mech 2000;67:819-822.
17. Kim JH, Paulino GH. Isoparameteric graded finite elements for nonhomogeneous isotropic and orthotropic materials. J Appl Mech 2002;69:502-514.
18. Kim JH, Paulino GH. Finite element evaluation of mixed-mode stress intensity factors in functionally graded materials. Int J Numer Meth Eng 2002;53:1903-1935.
19. Kim JH, Paulino GH. T-stress, mixed-mode stress intensity factors, and crack initiation angles in functionally graded materials: a unified approach using the interaction integral method. Comp Meth Appl Mech Eng 2003;192:1463-1494.

20. Dolbow JE, Gosz M. On the computation of mixed-mode stress intensity factors in functionally graded meterials. Int J Solids Struct 2002;39:2557-2574.

21. Chen J, Wu L, Du S. Element free Galerkin methods for fracture of functionally graded materials. Key Eng Mater 2000;183-187:487-492.

22. Rao BN, Rahman S. Mesh-free analysis of cracks in isotropic functionally graded materials. Eng Fract Mech 2003;70:1-27.

23. Yue ZQ, Xiao HT, Tham LG. Boundary element analysis of crack problems in functionally graded materials. Int J Solids Struct 2003;40:3273-3291.

24. Zhang Ch, Sladek J, Sladek V. Numerical analysis of cracked functionally graded materials. Key Eng Mater 2003;251-252:463-472.

25. Zhang Ch, Sladek J, Sladek V. Effects of material gradients on transient dynamic mode III SIFs in a FGM. Int J Solids Struct 2003;40:5251-5270.

26. Zhang Ch, Sladek J, Sladek V. Antiplane crack analysis of a functionally graded material by a BIEM. Comp Mater Sci 2005;32:611-619.

27. Zhang Ch, Sladek J, Sladek V. Transient dynamic analysis of cracked functionally graded materials. In:: Aliabadi MH et al., editors. Advances in Fracture and Damage Mechanics IV. Copyright EC, Ltd., United Kingdom, 2005, pp. 301-308.

28. Sladek J, Sladek V, Zhang Ch. An advanced numerical method for computing elastodynamic fracture parameters in functionally graded materials. Comp Mater Sci 2005;32:532-543.

29. Sladek J, Sladek V, Zhang Ch. A meshless local boundary integral equation method for dynamic anti-plane shear crack problem in functionally graded materials. Eng Anal Bound Elem 2005;29:334-342.

30. Sladek J, Sladek V, Zhang Ch. The MLPG method for crack analysis in anisotropic functionally graded materials. Struct Integr & Dur 2005;1:131-143.

31. Sladek J, Sladek V, Zhang Ch, Tan CL. Evaluation of fracture parameters for crack problems in FGM by a meshless method. J Theoret Appl Mech 2006;44:603-636.

32. Martin PA, Richardson JD, Gray LJ, Berger JR. On Green's function for a three-dimensional exponentially-graded elastic solid. Proc Royal Soc London A 2002;458:1931-1947.

33. Chan YS, Gray LJ, Kaplan T, Paulino GH. Green's function for a two-dimensional exponentially-graded elastic medium. Proc Royal Soc London A 2004;460:1689-1706.

34. Gao XW. The radial integration method for evaluation of domain integrals with boundary-only discretization. Eng Anal Bound Elem 2002;26:905-916.

35. Gao XW. A boundary element method without internal cells for two-dimensional and three-dimensional elastoplastic problems. J Appl Mech 2002;69:154-160.

36. Gao XW, Davies TG. Boundary element programming in mechanics. Cambridge: Cambridge University Press, 2002.

37. Nardini D, Brebbia CA. A new approach for free vibration analysis using boundary elements. In: Brebbia CA, editor, Boundary element methods in engineering, Berlin: Springer, 1982, pp. 312–326.

38. Golberg MA, Chen CS, Bowman H. Some recent results and proposals for the use of radial basis functions in the BEM. Eng Anal Bound Elem 1999;23:285-296.

39. Aliabadi MH. The boundary element method, Volume 2, Applications in solids and structures. John Wiley & Sons, 2002.

40. Zhang Ch, Gao X-W, Sladek J, Sladek V. Fracture mechanics analysis of 2-D FGMs by a meshless BEM. Key Eng Mater 2006;324-325:1165-1172.

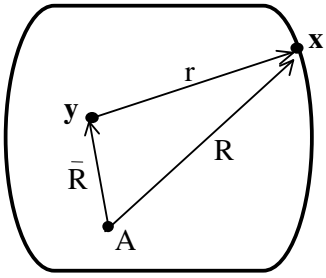

Fig. 1: Relationship between distances

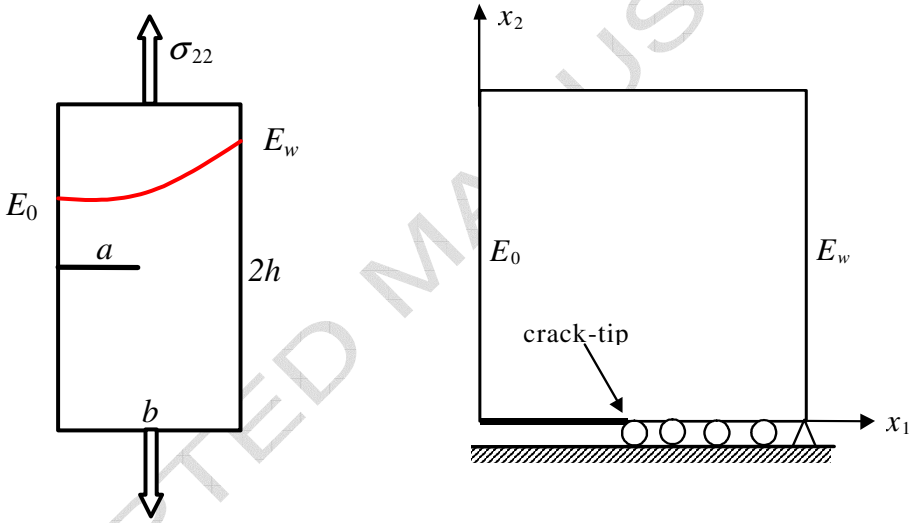

Fig. 2: An edge crack parallel to the material gradation in a rectangular functionally graded plate subjected to a tensile loading

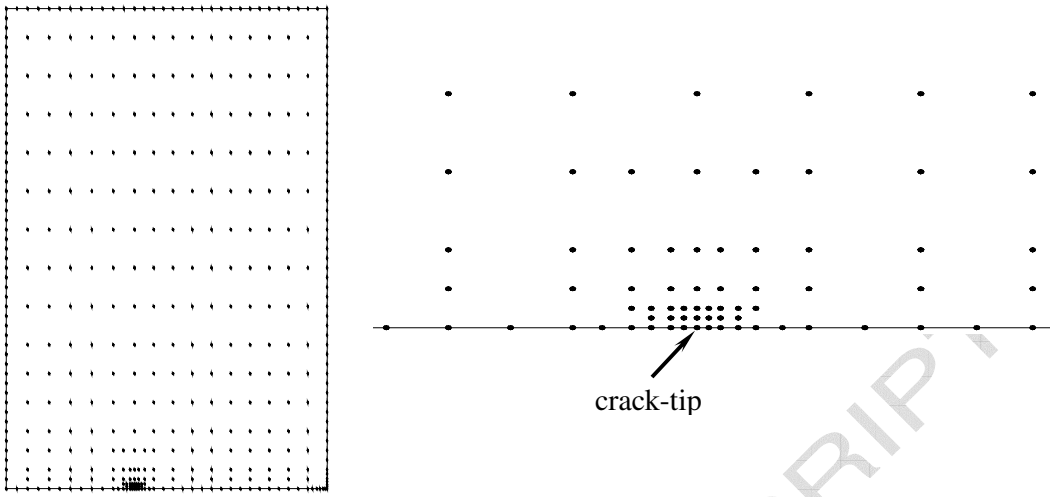

Fig. 3: Boundary and internal nodes (180 boundary nodes and 251 internal nodes)

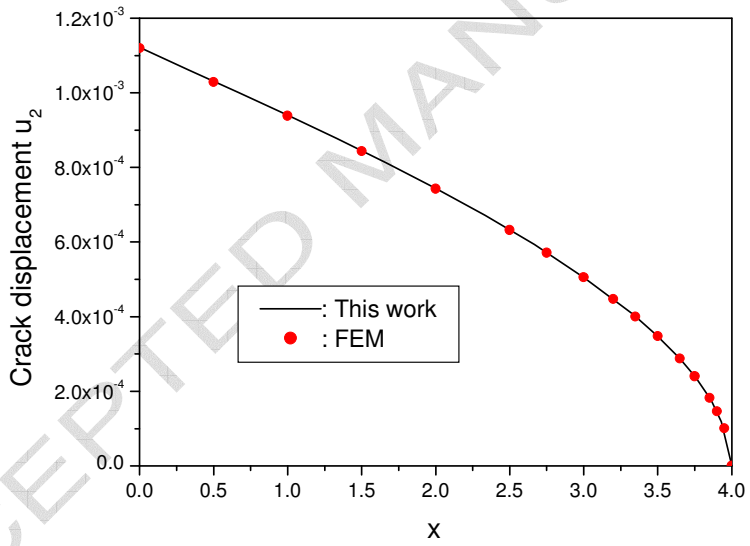

Fig. 4: Displacement component u_2 on the crack-face

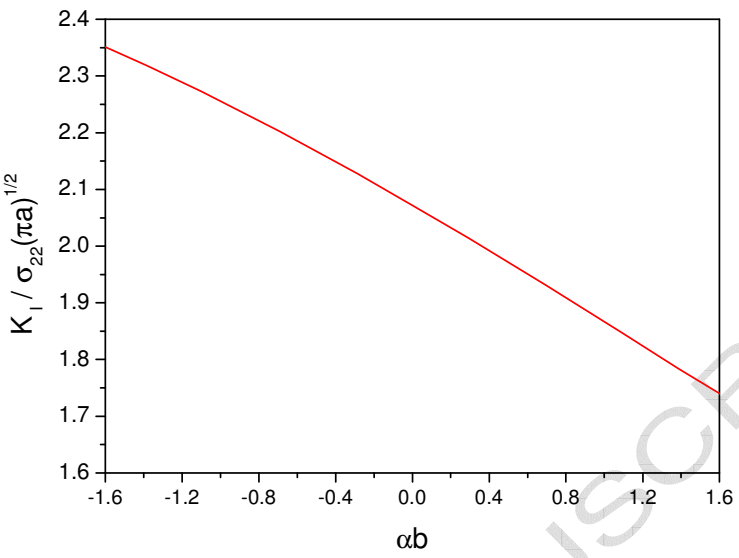

Fig. 5: Normalized mode-I stress intensity factor versus the dimensionless gradient parameter αb

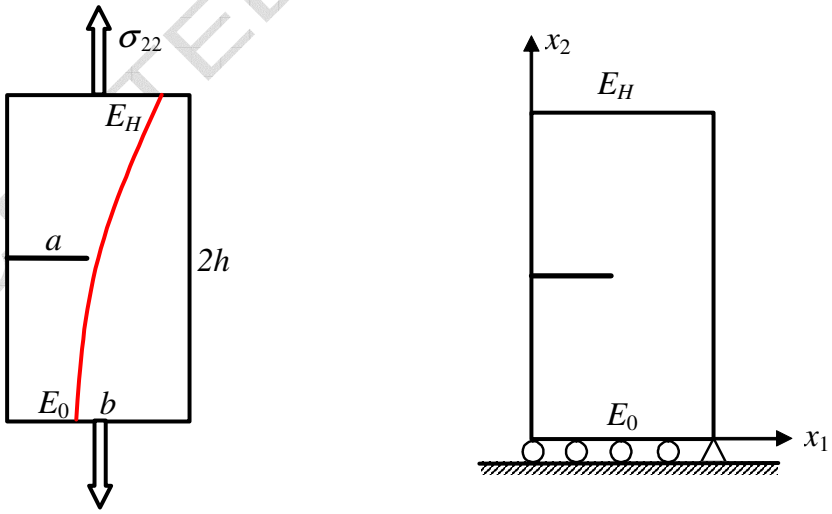

Fig. 6: An edge crack perpendicular to the material gradation in a rectangular functionally graded plate subjected to a tensile loading

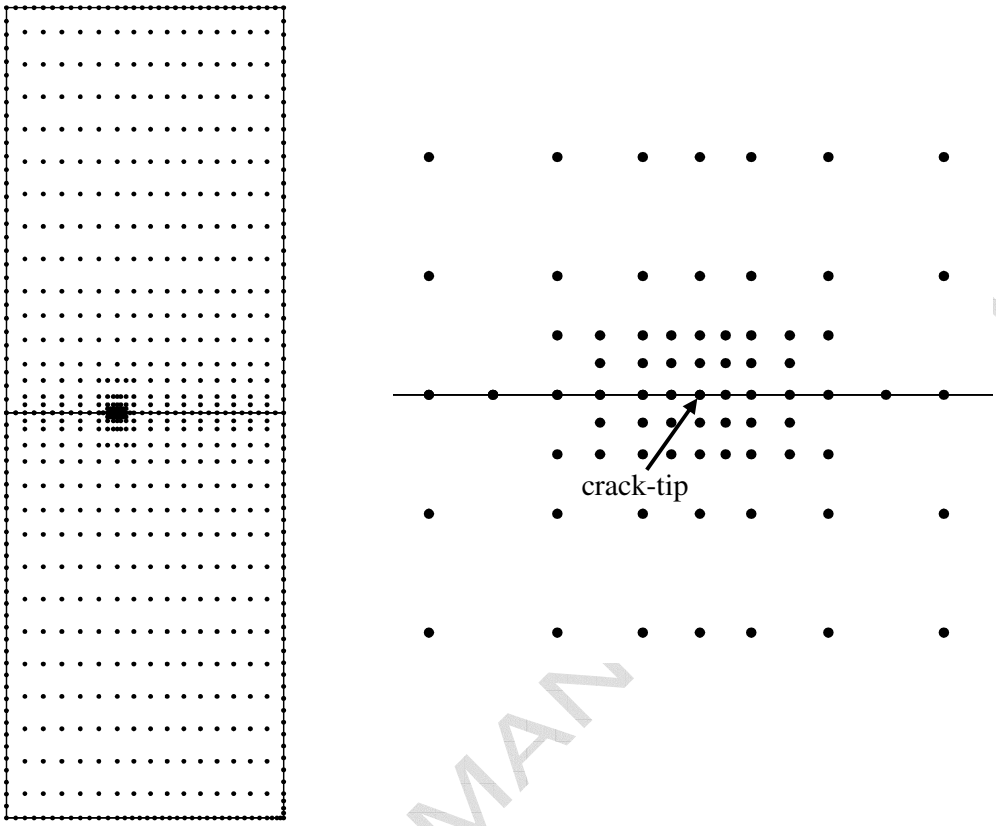

Fig. 7: Boundary and internal nodes (254 boundary nodes and 502 internal nodes)

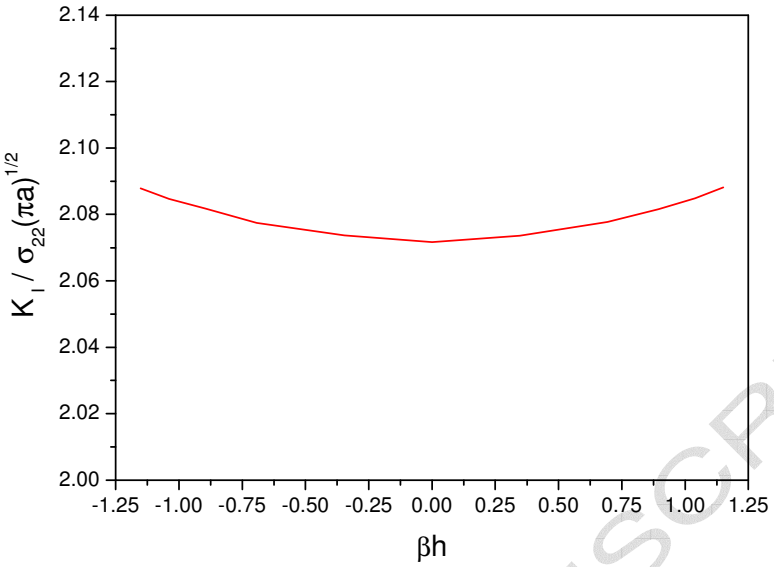

Fig. 8: Normalized mode-I stress intensity factor versus the dimensionless gradient parameter βh

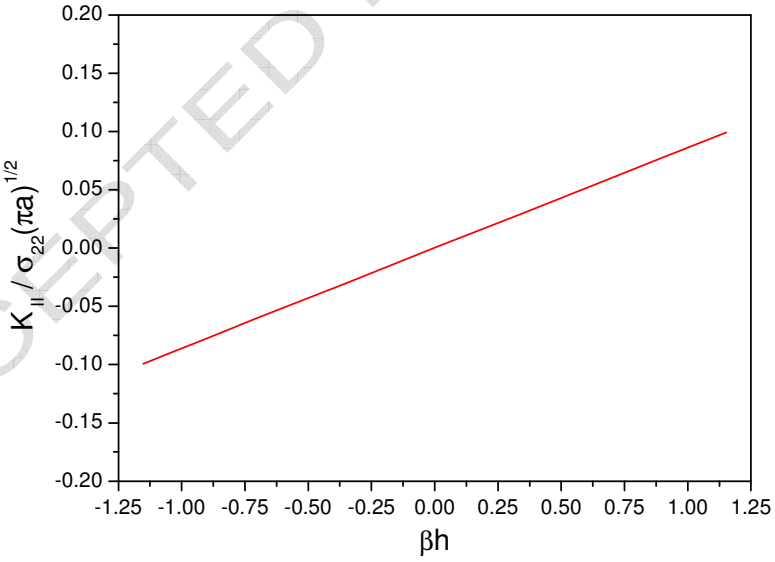

Fig. 9: Normalized mode-II stress intensity factor versus the dimensionless gradient parameter βh